Korean J. Chem. Eng., **22**(5), 762-769 (2005)

Ion Dynamics in Plasma Processing for the Fabrication of Ultrafine Structures

Chang-Koo Kim†

Department of Chemical Engineering, Ajou University, Suwon 443-749, Korea
(*Received 21 January 2005 • accepted 11 May 2005*)

Abstract−The flux, energy and angular distribution of ions generated from inductively coupled argon plasma were measured, using a gridded retarding field ion analyzer, to investigate the dynamics of ions in the plasma. The ion flux and the ion density at the sheath edge were found to increase with power, but to decrease with pressure. The ion energy was modulated, showing two peaks in the argon plasma, because the ratio of the ion transit time to the rf period was less than or comparable to unity. The peak, mean, minimum, and maximum ion energy decreased with increasing pressure, but were nearly constant as power was varied. The ion angular distributions had a Gaussian distribution peaked at zero angle from surface normal. The full-width-at-half-maximum was increased with increasing both power and pressure. The ion temperature was readily obtained from the ion angular distributions, and the value was in the range of 0.08-0.14 eV, agreeing with typical ion temperature values measured previously in inductively coupled plasmas.

Key words: Plasma, Ion Energy Distribution, Ion Angular Distribution, Ion Dynamics, Ion Analyzer

INTRODUCTION

Etching and deposition of thin solid films are central unit operations in the fabrication of various devices such as integrated circuit (IC) devices, microelectromechanical (MEMS) devices, and photonic devices. Plasmas are widely used in etching and deposition processes due to their capabilities for low-pressure operation and anisotropic pattern fabrication [Hwang et al., 2003; Ryu et al., 2003; Chung et al., 2002; Cho et al., 2000]. The etch rate (or deposition rate), selectivity, and anisotropy of patterns are directly affected by the flux, energy, and direction of ions impinging on a substrate. Therefore, measurements of the flux, energy and angular distributions of ions generated from a plasma are of primary importance for understanding ion dynamics during plasma processing. Furthermore, an increase in the utility of high density plasmas (e.g., inductively coupled plasma) makes it more important to study energy and angular distributions of ions incident on the substrate.

Theoretical and experimental works on the energy and angular distributions of ions in direct current (dc) plasmas [Ingram and Braithwaite, 1990], capacitively coupled radio frequency (rf) plasmas [Kortshagen and Zethoff, 1995; Flender and Wiesemann, 1994; Liu et al., 1990; Ingram and Braithwaite, 1988], and inductively coupled rf plasmas [Woodworth et al., 1996, 1997; Holber and Forster, 1990] have been extensively published since the 1970s. Ingram and Braithwaite [1988] studied the energy distributions of Ar ions bombarding a grounded electrode of a capacitively coupled rf discharge. They also investigated the energy distributions of Ar ions in a filament-assisted dc plasma generated between parallel electrodes and studied the modulation of the plasma potential by applying various frequencies of rf power to one electrode [Ingram and Braithwaite, 1990]. They observed that the ion energy distribution responds to the modulation of the plasma potential when the rf period is longer than the ion transit time. Flender and Wiesemann [1994] studied the ion energy distributions on the grounded electrode of a capacitively coupled rf discharge in a wide range of pressure (0.001-0.1 mbar) in different gases (Ar, O_2, He). At lower pressures (~0.03 mbar), a double-peak structure of the ion energy distribution was resolved due to the transition from a collisional sheath to collisionless sheath.

Recently, many studies on the energy distributions of ions in inductively coupled plasmas have been reported. Kortshagen and Zethoff [1995] measured the energy distributions of Ar ions on the grounded electrode of a planar inductively coupled plasma. They found structured distributions when the inductive discharge had a considerable parasitic capacitive coupling from the induction coil, and single peaks with energies below 20 eV when this parasitic capacitive coupling was removed. Woodworth et al. [1996, 1997] studied extensively the ion energy distributions on the grounded electrode of an inductively coupled plasma in a variety of gases (Ar, Cl_2).

While the ion energy distributions have been widely studied, very few measurements have been reported on ion angular distributions in plasmas. Liu et al. [1990] measured for the first time the angular distributions of Ar ions in a capacitively coupled rf plasma. They showed that 30% of the ions have incident angles greater than 10° from the surface normal at 10 mtorr. This fraction increases as the pressure is increased and ions are scattered in the sheath by collisions. Woodworth et al. [1996, 1997] presented the ion angular distributions in Ar and Cl_2 plasmas using an inductively coupled plasma source, and found that the width of the distributions increases with both power and pressure. Aydil et al. [1998] also measured the ion angular distributions in Ar plasma using a helicon plasma source. They proposed that the width of the ion angular distribution is determined by the ratio of the directed ion energy gained in the sheath to the random ion energy in the plasma.

Gridded retarding field ion analyzers are used routinely to measure the energy and angular distributions of ions because of their simple concept and operation. Theoretical and experimental works have been published on the design and performance of gridded retarding field ion analyzers [Woodworth et al., 1997, 1996; Flender and Wiesemann, 1994; Bohm and Perrin, 1993; Liu et al., 1990;

†To whom correspondence should be addressed.
E-mail: changkoo@ajou.ac.kr

Ingram and Braithwaite, 1988]. Ion analyzers can be pumped differentially to minimize ion-neutral collisions inside the analyzer [Woodworth et al., 1996, 1997; Flender and Wiesemann, 1994; Liu et al., 1990]. Differential pumping is not necessary if the distance an ion travels in the analyzer before arriving at a collecting electrode is greater than the mean free path of the ion [Bohm and Perrin, 1993; Ingram and Braithwaite, 1988]. Bohm and Perrin [1993] discussed the influence of ion analyzer geometry on the measured current-voltage (I-V) characteristic. They also discussed problems arising from poor analyzer design, potential distributions between the grids, intergrid distance, and the mesh size. Ingram and Braithwaite [1988] referred to the necessity of focusing ions after passing through an orifice. The grid alignment was found to affect greatly the energy resolution of the analyzer [Woodworth et al., 1996]. Grids non-parallel to each other will reduce the analyzer resolution. Thus, it is favored to spot weld the grids on adequate supports.

In this work, the flux, energy and angular distribution of ions generated from an inductively coupled argon plasma were measured with a gridded retarding field ion analyzer. Based on these measurements, ion properties such as ion density, mean ion energy, and ion temperature were easily obtained, thus helping one to understand the dynamics of ions in an inductively coupled plasma.

EXPERIMENTAL

1. Plasma Source

An inductively coupled high-density plasma was used in this study. Fig. 1 shows the schematic of a plasma source equipped with a gridded retarding field ion analyzer. The plasma was ignited in a ceramic tube (Al_2O_3) with 31.75 mm in inner diameter and 82.55 mm in length, by applying 13.56 MHz rf power to a three-turn coil through a matching network. A stainless steel electrode was placed at the bottom of the source and kept grounded during the experiments. The stainless steel electrode had a pinhole, whose diameter was 10 μm and thickness was 2.5 μm, to sample ions from the plasma.

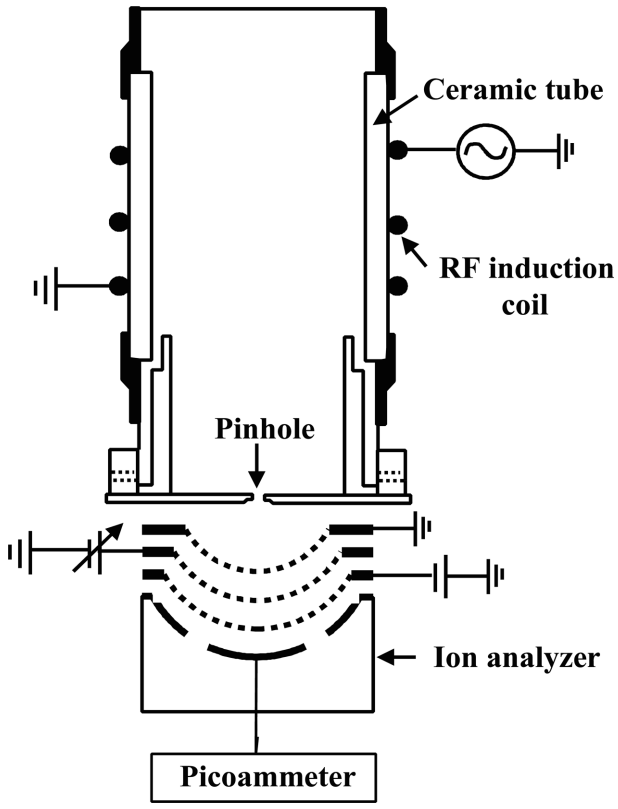

Fig. 1. Schematic of the plasma source equipped with a gridded retarding field ion analyzer.

Argon was selected as a discharge gas since its simple plasma chemistry makes it an appropriate starting gas for understanding the ion dynamics. The pressure and the power ranged 5-50 mtorr and 200-600 W, respectively. The plasma source was mounted on an ultrahigh vacuum (UHV) chamber. During experiments (with a gas flowing into the plasma), a pressure of about 1×10^{-5} Torr was routinely achieved in the UHV chamber.

2. Gridded Retarding Field Ion Analyzer

A gridded retarding field ion analyzer was located behind the pinhole electrode (grounded) to measure the flux, energy and angular distribution of ions striking the pinhole electrode. The ion analyzer consisted of three screens and 11 annular current collecting electrodes. All screens and collecting electrodes are shaped as part of concentric hemispheres centered at the pinhole. The collecting electrodes were electrically isolated by epoxy between them so that each electrode was 2-3° wide.

Table 1 shows the area of each collecting electrode. Electrode number 1 and electrode number 11 represent the center (surface normal) and the outermost electrode, respectively. It can be seen that the area of each collecting electrode varies by more than a factor of 70 as one moves from the smaller electrode at the center to the largest electrode at the edge of the ion analyzer. Therefore, it is necessary to divide the raw signals from each electrode by the electrode area for the measurement of ion angular distributions.

The hemispherical screens were mounted on the stainless steel screen holders by holding them between a hemispherical brass mandrel and the screen holders, and spot welding them following Taylor [1988]. Great care was taken to make the screens hemispherical. Ingram and Braithwaite [1988] have discussed that defocusing fields between a hole and a collecting electrode would cause measurement errors.

The top screen (closest to the pinhole) and the bottom screen (closest to the collecting electrodes) were 50 lines per inch with 0.0254 mm wire diameter and 0.4826 mm square openings, and had 90%

Table 1. Area of each collecting electrode of the ion analyzer

Electrode number	Electrode area (mm^2)
1	4.2
2	10.8
3	15.8
4	24.1
5	29.6
6	32.4
7	55.4
8	41.0
9	82.0
10	94.4
11	304.8

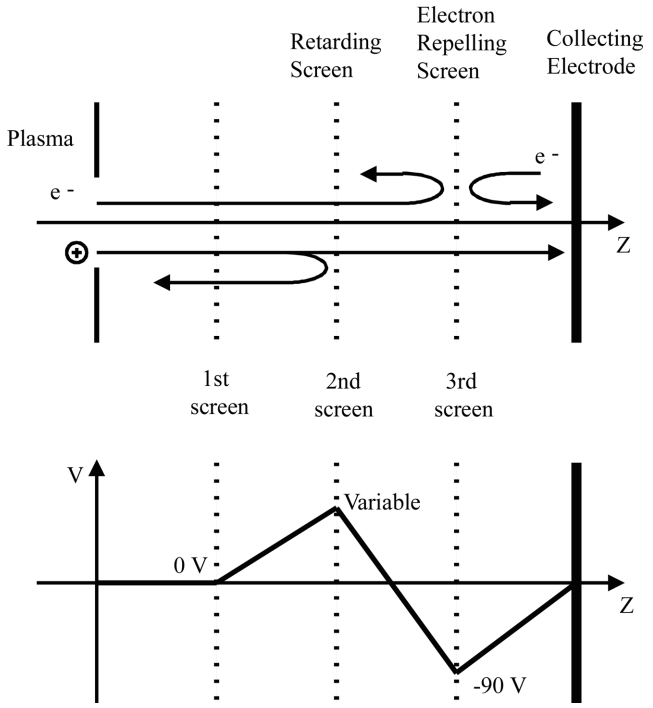

Fig. 2. Simplified illustration of the operation of the gridded retarding field ion analyzer (top) and potential distributions along the analyzer axis (bottom).

transparency. The middle screen was 100 lines per inch with 0.0254 mm wire diameter and 0.2286 mm square openings, and was 81% open. All screens were made of stainless steel. Four Teflon spacers were inserted between each pair of screen holders (12 spacers total) to electrically isolate them. The assembly of the ion analyzer produced a distance of 27.9 mm from the hole to the collecting electrodes.

MEASUREMENTS AND DATA ANALYSIS

1. Gridded retarding Field Ion Analyzer

A gridded retarding field ion analyzer consists of a set of grids (screens) at different potentials and collecting electrodes. Fig. 2 represents a simplified illustration of the operation of the gridded retarding field ion analyzer located behind an aperture (hole) next to a plasma. When a plasma is struck above the hole, electrons and positive ions are extracted through the hole. The first screen is maintained at the same potential as the hole to create a field-free region between the hole and the ion analyzer. Hence, the ion path after the ion penetration through the hole is preserved. If the second screen (ion retarding screen) were set to a certain positive potential with respect to the hole, only ions with energies greater than the second screen potential would pass through the screen and detected by the collecting electrode. The third screen (electron repelling screen) is biased at a negative potential with respect to the hole for two reasons. First, electrons from the plasma are prevented from reaching the collecting electrodes. This implies that the negative bias on the third screen has to be larger (in absolute value) than the sheath potential over the hole. Second, secondary electrons emitted from the collecting electrode are repelled back to the electrode. If these secondary electrons escaped the collecting electrode, a spuriously higher ion current would be measured.

2. Ion Flux Measurement

Using the ion analyzer described in the above section, ion flux measurements were conducted. The top screen was grounded to have the same potential as the pinhole. The bottom screen was biased at −90 V. The middle screen was set to zero voltage to allow all ions passing through the pinhole to reach the collecting electrode. The ion flux was obtained by dividing the total current by the pinhole area after the transmissions of the screens were accounted for, i.e., the measured current was divided by 0.81×0.9×0.81.

3. Measurement of the Ion Energy Distribution

To obtain the ion energy distribution, the middle screen was swept from zero (ground) to positive voltages at intervals of 1 V until the measured current was zero. The first and the third screens of the ion analyzer were also set at zero and −90 V, respectively, with respect to the pinhole. Five current measurements were taken at each voltage on the middle screen and averaged to obtain one data point. The ion energy distribution function, f, was obtained by differentiating the current, I_i, with respect to voltage on the middle screen, V_m, or

$$f(V_m) = -\frac{dI_i(V_m)}{dV_m}. \quad (1)$$

The mean ion energy, $\overline{E}$, was obtained from the ion energy distribution function as

$$\overline{E} = \frac{\int_0^\infty E f(E) dE}{\int_0^\infty f(E) dE}. \quad (2)$$

Assuming perfectly flat screens, the energy resolution (ΔE/E) of an ion analyzer is limited by the finite hole size of the middle screen (ion retarding screen) and the distance between the middle screen and the adjacent screens. Sakai and Katsumata [1985] studied the influence of geometrical factors on the energy resolution of a retarding field electrostatic analyzer made of three screens by approximating each screen with a single hole. They derived an expression for the energy resolution as

$$\frac{\Delta E}{E} = \frac{\alpha s}{2\pi l}\left(1+\frac{d}{\alpha s}+\frac{d}{2\alpha^2 s^2}\right)\left[1+\frac{2d}{\alpha s}\tan^{-1}\left(\frac{d}{\alpha s}\right)-\frac{2d}{\alpha s}\tan^{-1}\left(\frac{2d}{\alpha s}\right)\right], \quad (3)$$

where α=1.13, d is the diameter of the screen wire, s is the spacing between wires, and l is the distance between screens. Based on Eq. (3) and the geometrical parameters of the ion analyzer used in this work (d=0.0254 mm, s=0.2286 mm, and l=2.159 mm), the energy resolution is estimated to be about 3%.

4. Measurement of the Ion Angular Distribution

To measure the ion angular distributions, the top and bottom screens were again maintained at zero and −90 V, respectively. The middle screen was set to 0 V to allow all ions to reach the collecting electrodes. An ion will hit one of the collecting electrodes according to its angle coming out of the hole. Thus, measurement of the ion current at each collecting electrode gave the ion angular distribution. Five current measurements were taken at each electrode and averaged to obtain one data point.

Due to the finite thickness of the hole, an ion incident normal to the hole plane "sees" a greater opening than an ion approaching at an off-normal angle. This effect was corrected following Liu et al.

[1990]. Based on their work, the fraction of ions, passing through a hole, that do not strike the inner walls of the hole, f_i, is expressed as

$$f_i = 1 - \frac{(t/R)\tan\theta(4-(t/R)^2\tan^2\theta)^{1/2}}{\pi} - \frac{\phi - \sin\phi}{\pi}, \quad (4)$$

where

$$\phi = 2\sin^{-1}\left(\frac{t\tan\theta}{2R}\right). \quad (5)$$

In Eqs. (4) and (5), θ is the angle from the surface normal, t is the hole thickness, and R is the hole radius. It can be seen that an ion at normal incidence (θ=0°) or in the case of an infinitely thin orifice (t=0) make f_i unity. For a 10 μm-diameter pinhole (2.5 μm thick), ions incident at 34° from the surface normal (the maximum ion angle that can be captured by the ion analyzer used in this work) see only 79% of the open hole area.

RESULTS AND DISCUSSION

1. Ion Flux

Fig. 3 shows the total ion flux measured as a function of pressure and power in an argon plasma. The ion flux increases with plasma power at a given pressure. This is expected since the plasma density increases approximately linearly with power. The ion flux decreases with increasing argon pressure, which is contrary to our expectation but can be interpreted as the following. As gas pressure increases, the electron temperature decreases [Schwabedissen et al., 1997]; consequently, the Bohm velocity of ions is lowered. Also, higher pressures result in stronger ion density gradients. Both effects tend to lower the ion flux out of the plasma.

Measurements of ion flux allow one to calculate the ion density at the sheath edge. Using the Bohm sheath criterion, the ion density at the sheath edge, n_{is}, can be calculated by the assumption of collisionless sheath, i.e., the ion flux is constant in the sheath [Chapman, 1980].

$$n_{is} = \frac{J}{eu_B}. \quad (6)$$

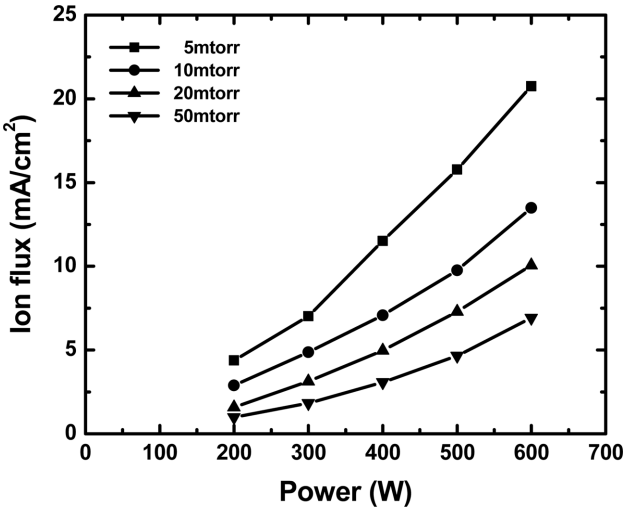

Fig. 3. Total ion flux measured in argon plasma as a function of power and pressure.

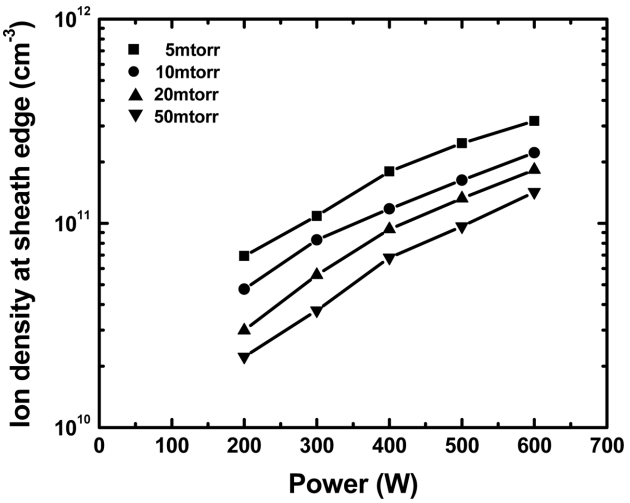

Fig. 4. Ion density at the sheath edge over the pinhole in an argon plasma as a function of power at various discharge gas pressures.

In Eq. (6), J is the ion flux, e is the charge of the electron, and u_B is the Bohm velocity defined as

$$u_B = \left(\frac{kT_e}{m_i}\right)^{1/2}, \quad (7)$$

where k is the Boltzmann constant, T_e is the electron temperature, and m_i is the ion mass.

Fig. 4 shows the ion density at the sheath edge in an argon plasma as a function of power at various pressures. The ion density at the sheath edge increases with power but decreases with pressure as in the case of ion flux.

2. Ion Energy Distributions

Fig. 5 shows the energy distributions of ions as a function of power and pressure in an argon plasma. At a constant pressure, the peak, minimum, and maximum ion energy are nearly constant as power is varied. This behavior is consistent with other studies in argon or other discharges [Wooldworth et al., 1996, 1997; Kortshagen and Zethoff, 1995]. It is a characteristic of ion energy distributions in inductively coupled plasmas. In these plasmas, plasma power controls ion flux, not ion energy. In other words, the plasma potential is not controlled by the source power so that ion energy is nearly independent of the source power. At constant power, the peak, minimum and maximum ion energy decreased as pressure was increased in all cases. It is expected that ions will experience more collisions with increasing pressure, resulting in lower ion energy.

It is seen that the ion energy distributions have double peaks in argon plasmas. The shape of the ion energy distribution in an rf sheath depends critically on the product of the ion transit time (τ_i) and the angular frequency of the applied field (ω) [Panagopoulos and Economou, 1999]. When $\omega\tau_i \ll 1$, ions cross the sheath in a short time compared to the field oscillations. Under this condition, the ion energy will depend on the phase of the rf cycle when the ion enters the sheath. Thus, ion energy distributions are doubly peaked with the maximum and minimum energies corresponding to ions crossing the sheath during the maximum and minimum sheath potential, respectively. On the other hand, when $\omega\tau_i \gg 1$, ions experience many

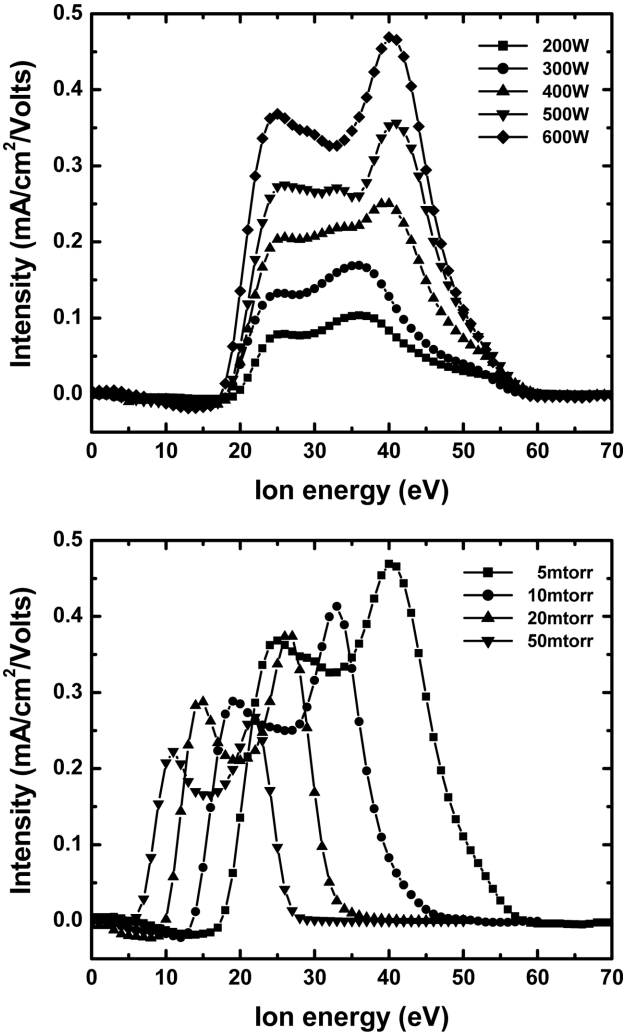

Fig. 5. Energy distributions of ions in an argon plasma: (a) 5 mtorr pressure (top) and (b) 600 W power (bottom).

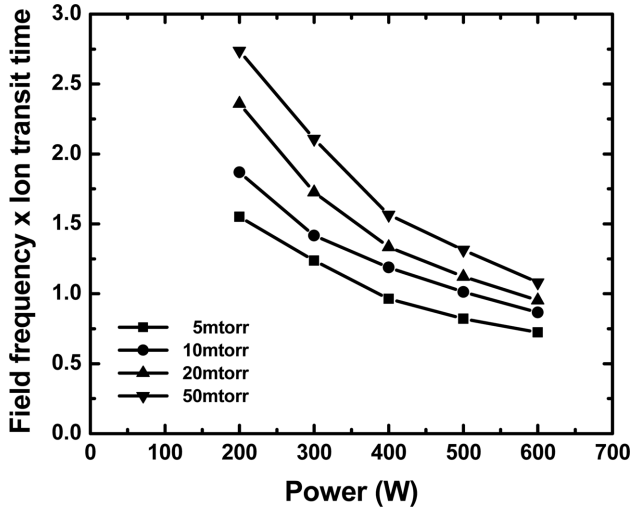

Fig. 6. Product of the field frequency (ω) and ion transit time (τ_i) as a function of power at various argon gas pressures.

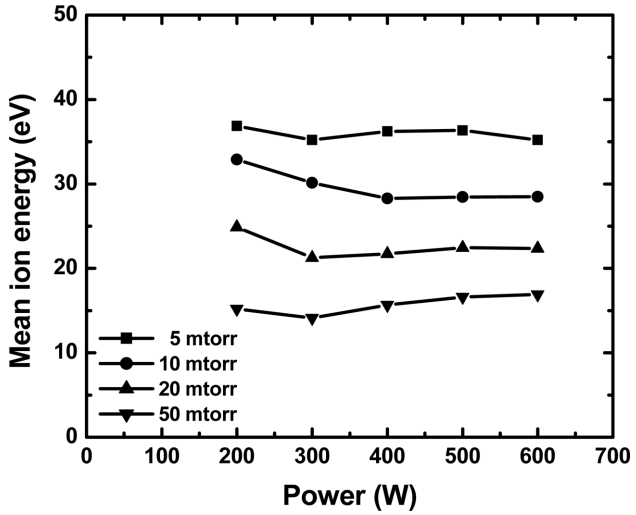

Fig. 7. Mean ion energies in an argon plasma.

field oscillations while crossing the sheath. The ion energy will then depend on the average sheath potential, resulting in a single peak in the ion energy distributions.

For an unbiased sheath, the ion transit time is equal to the inverse of the ion plasma frequency (ω_{pi}) based on the plasma density at the sheath edge [Panagopoulos and Economou, 1999],

$$\tau_i = 1/\omega_{pi}, \tag{8}$$

where

$$\omega_{pi} = \left(\frac{e^2 n_{is}}{\varepsilon_0 m_i}\right)^{1/2}. \tag{9}$$

In Eq. (9), ε_0 is the permittivity of the free space.

Fig. 6 shows the product of the angular frequency of the applied field and the transit time of ions in an argon plasma. A 13.56 MHz field was applied so that the angular frequency is $(2\pi)\times(13.56\,\text{MHz}) = 8.52\times10^7\,\text{s}^{-1}$. It can be seen that $\omega\tau_i$ is about 0.7-2.7 over the range of power and pressure applied in this work. Ulacia and McVittie [1989] pointed out that the modulation of ion energy is still apparent even when the ion transit time is about five rf periods. Thus, it can be concluded that the energy of ions impinging on the electrode should be modulated. In Fig. 5, all ion energy distributions obtained in an argon plasma show double peaks, implying that the ion transit time is smaller than, or not much larger than, the rf period for this pressure and power range.

The mean ion energy was obtained by integrating the ion energy distribution function. Fig. 7 shows mean ion energies in argon discharge as a function of power and pressure. The mean ion energies are nearly constant with power, and decrease with increasing pressure. This is consistent with other studies of inductively coupled plasmas, in which only plasma power weakly affects the mean ion energy [Woodworth et al., 1996; Kortshagen and Zethoff, 1995; Holber and Forster, 1990]. This is in contrast to capacitively coupled plasmas, in which the mean ion energy typically varies linearly with the rf peak-to-peak voltage.

Mean ion energies measured in this experiment are a bit higher than those obtained other studies of inductively coupled argon plasmas [Woodworth et al., 1996; Kortshagen and Zethoff, 1995; Hol-

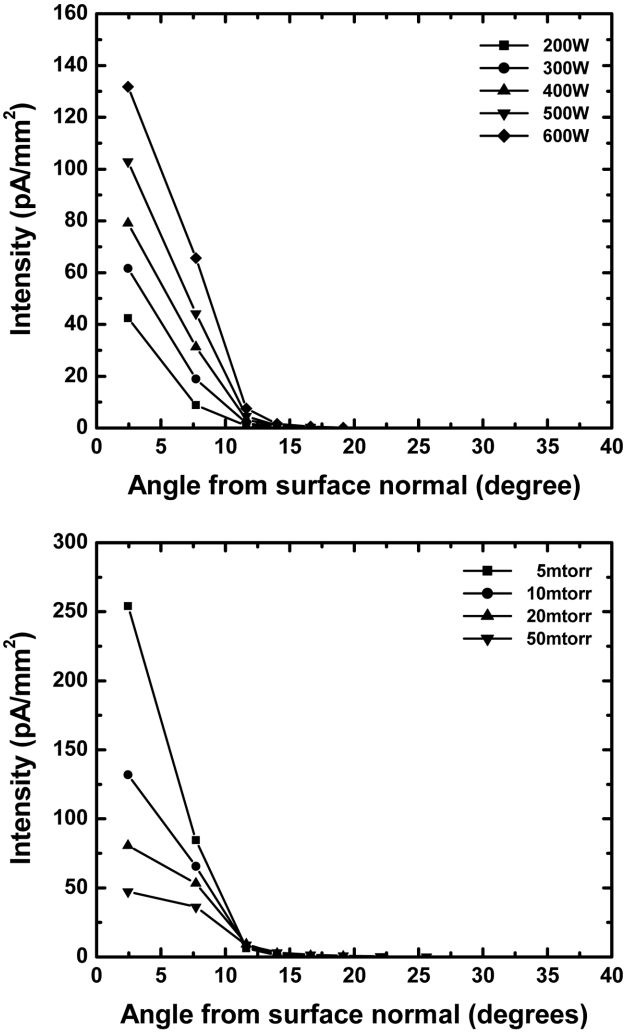

Fig. 8. Angular distributions of ions in an argon plasma: (a) 10 mtorr pressure (top) and (b) 600 W power (bottom). Ion currents on each collecting electrode were divided by the electrode area.

ber and Forster, 1990]. The most likely source of this effect is stray capacitive coupling from the unshielded coil to the plasma. Capacitive coupling was approximately constant and did not increase, for example, with increasing power to the plasma.

3. Ion Angular Distributions

Fig. 8 shows the ion angular distributions in an argon plasma. All ion angular distributions have a Gaussian shape peaked at the center electrode as pressure and power are varied. Because the distributions are Gaussian, the effect of pressure and power can be investigated by using the full-width-at-half-maximum (FWHM). For Gaussian distributions, the ion angular distribution function (f_θ) is given by [Gottscho, 1993]

$$f_\theta = C_N \exp(-\beta\theta^2), \tag{10}$$

where C_N is a normalization constant, θ is the incidence angle measured from the surface normal, and β is the ratio of the directed energy gained in the sheath (sheath potential, V_{sh}) to the random ion energy (related to the ion temperature, T_+) in the plasma. The parameter β determines the FWHM of the ion angular distribution

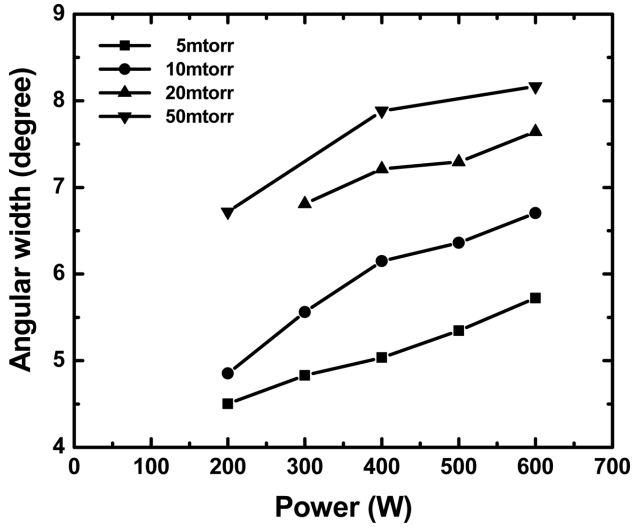

Fig. 9. Full-width-at-half-maximum (FWHM) of ion angular distributions in an argon plasma as a function of power and pressure.

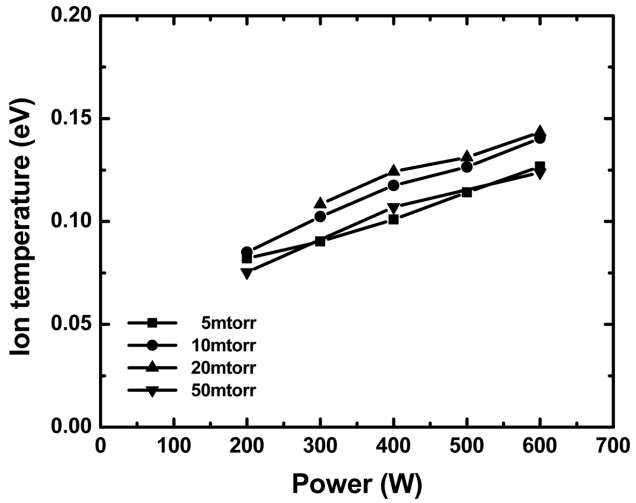

Fig. 10. Ion temperature in an argon plasma as a function of power at various pressures.

$$\Delta\theta_{FWHM} = 2\sqrt{\frac{\ln 2}{\beta}}, \tag{11}$$

where

$$\beta = \frac{eV_{sh}}{kT_+}. \tag{12}$$

Fig. 9 shows the FWHM of the ion angular distributions as a function of pressure and power. At given power, the FWHM increases as pressure is increased. Increasing pressure will broaden the FWHM through collisions with neutrals. The FWHM also increases as power is increased at a given pressure. The dependence of the ion temperature on power is complex but, in general, the ion temperature increases with power [Aydil et al., 1998; Hebner, 1996; O'Neill et al., 1993]. Now, the directed energy of ions is nearly constant with plasma power because the plasma potential is nearly independent of power. The FWHM, therefore, increases as power is increased

in the case of the unperturbed plasma.

From the measured sheath potential (mean ion energy) and the FWHM of the ion angular distribution, the ion temperature (T_+) can be estimated by using Eqs. (11) and (12). Fig. 10 shows the estimated ion temperature in an argon plasma as a function of power at various gas pressures. As expected, the ion temperature increases with power. Ion temperatures are in the range of 0.08-0.14 eV, which are fairly consistent with ion temperatures measured by Fabry-Perot interferometry [O'Neill et al., 1993] and laser-induced fluorescence [Hebner, 1996] in inductively coupled argon plasmas.

CONCLUSIONS

The ion dynamics in an inductively coupled argon plasma was investigated by measuring the flux, energy and angular distributions of ions generated from the plasma. The measurements were made by using a gridded retarding field ion analyzer, and these measurements allowed one to easily obtain ion properties such as ion density, mean ion energy, and ion temperature.

The ion flux and the ion density at the sheath edge increased with power, but decreased with pressure, because of stronger density gradients at higher pressures.

The ion energy distribution had two peaks in an argon plasma. The ion energy was modulated in this case, because the ion transit time through the sheath was smaller than or comparable to the rf period. The peak, minimum, and maximum ion energy were nearly constant as power was varied. This is because, in inductively coupled plasmas, plasma power controls ion flux, not ion energy. The peak, minimum, and maximum ion energy decreased with increasing pressure since ions experienced more collisions with neutrals with increasing pressure. The mean ion energy, which was obtained from the ion energy distribution, was nearly constant with power, and decreased with increasing pressure.

The ion angular distribution had a Gaussian shape peaked at zero angle from surface normal in an argon plasma. The full-width-at-half-maximum (FWHM) was increased with increasing power since the ratio of the directed ion energy gained in the sheath (sheath potential) to the random ion energy (ion temperature) in the plasma decreased with increasing power. The FWHM was also increased with pressure due to enhanced ion-neutral collisions at high pressures. The ion temperature was in the range of 0.08-0.14 eV, which agreed with typical ion temperature values previously measured in inductively coupled plasmas.

ACKNOWLEDGMENT

This work was supported by Korean Research Foundation Grant (KRF-2003-003-D00094).

NOMENCLATURE

C_N : constant
d : diameter of the screen wire
e : electron charge
$\overline{E}$: mean ion energy
f : ion energy distribution function
f_i : fraction of ions that do not strike the inner walls of the hole
f_θ : ion angular distribution function
I_i : ion current
J : ion flux
k : Boltzmann constant
l : distance between screens
m_i : ion mass
n_{is} : ion density at the sheath edge
R : hole radius
s : spacing between wires
t : hole thickness
T_e : electron temperature
T_+ : ion temperature
u_B : Bohm velocity
V_m : voltage on the middle screen
V_{sh} : plasma potential

Greek Letters

α : constant
β : ratio of the directed energy gained in the sheath to the random ion energy
ε_0 : permittivity of the free space
θ : angle from the surface normal
τ_i : ion transit time
ω : field frequency
ω_{pi} : plasma frequency

REFERENCES

Aydil, E. S., Quiniou, B. O. M., Lee, J. T. C., Gregus, J. A. and Gottscho, R. A., "Incidence Angle Distributions of Ions Bombarding Grounded Surfaces in High Density Plasma Reactors," *Mater. Sci. Semicond. Process.*, **1**, 75 (1998).

Bohm, C. and Perrin, J., "Retarding-Field Analyzer for Measurements of Ion Energy Distributions and Secondary Electron Emission Coefficients in Low-Pressure Radio Frequency Discharges," *Rev. Sci. Instrum.*, **64**, 31 (1993).

Chapman, B., *Glow Discharge Processes*, John Wiley & Sons, Inc., New York (1980).

Cho, B.-O., Ryu, J.-H., Hwang, S.-W., Lee, G. R. and Moon, S. H., "Direct Pattern Etching for Micromachining Applications without the Use of a Resist Mask," *J. Vac. Sci. Techol. B*, **18**, 2769 (2000).

Chung, C. W., Byun, Y. H. and Kim, H. I., "Inductively Coupled Plasma Etching of $Pd(Zr_xTi_{1-x})O_3$ Thin Films in Cl_2/C_2F_6/Ar and HBr/Ar Plasmas," *Korean J. Chem. Eng.*, **19**, 524 (2002).

Flender, U. and Wiesemann, K., "Ion Distribution Functions Behind an RF Sheath," *J. Phys. D: Appl. Phys.*, **27**, 509 (1994).

Gottscho, R. A., "Ion Transport Anisotropy in Low Pressure, High Density Plasmas," *J. Vac. Sci. Technol. B*, **11**(5), 1884 (1993).

Hebner, G. A., "Spatially Resolved, Excited State Densities and Neutral and Ion Temperatures in Inductively Coupled Argon Plasmas," *J. Appl. Phys.*, **80**, 2624 (1996).

Holber, W. M. and Forster, J., "Ion Energetics in Electron Cyclotron Resonance Discharge," *J. Vac. Sci. Technol. A*, **8**(5), 3720 (1990).

Hwang, S.-W., Lee, G.-R., Min, J.-H. and Moon, S. H., "Thickness of a Modified Surface Layer Formed in a Silsesquioxane-based Low-k Material During Etching in a Fluorocarbon Plasma," *Korean J. Chem. Eng.*, **20**, 1131 (2003).

Ingram, S. G. and Braithwaite, N. St. J., "Ion and Electron Energy Analysis at a Surface in an RF Discharge," *J. Phys. D: Appl. Phys.*, **21**, 1496 (1988).

Ingram, S. G. and Braithwaite, N. St. J., "RF Modulation of Positive-Ion Energies in Low-Pressure Discharges," *J. Appl. Phys.*, **68**(11), 5519 (1990).

Kortshagen, U. and Zethoff, M., "Ion Energy Distribution Functions in a Planar Inductively Coupled RF Discharge," *Plasma Sources Sci. Technol.*, **4**, 541 (1995).

Liu, J., Huppert, G. L. and Sawin, H. H., "Ion Bombardment in RF Plasmas," *J. Appl. Phys.*, **68**, 3916 (1990).

O'Neill, J. A., Barnes, M. S. and Keller, J. H., "Optical Ion Energy Measurements in a Radio-Frequency-Induction Plasma Source," *J. Appl. Phys.*, **73**, 1621 (1993).

Panagopoulos, T. and Economou, D. J., "Plasma Sheath Model and Ion Energy Distribution for All Radio Frequencies," *J. Appl. Phys.*, **85**, 3435 (1999).

Ryu, J.-H., Cho, B.-O., Hwang, S.-W., Moon, S. H. and Kim, C.-K., "Trajectories of Ions Inside a Faraday Cage Located in a High Density Plasma Etcher," *Korean J. Chem. Eng.*, **20**, 407 (2003).

Sakai, Y. and Katsumata, I., "An Energy Resolution Formula of a Three Plane Grids Retarding Field Energy Analyzer," *Jpn. J. Appl. Phys.*, **24**, 337 (1985).

Schwabedissen, A., Benck, E. C. and Roberts, J. R., "Langmuir Probe Measurements in an Inductively Coupled Plasma Source," *Phys. Rev. E.*, **55**, 3450 (1997).

Talyor, P. A., "Construction of Pierced Hemispherical Grids," *J. Vac. Sci. Technol. A*, **6**, 2583 (1988).

Ulacia, F. J. I. and McVittie, J. P., "A Two-Dimensional Computer Simulation for Dry Etching Using Monte Carlo Techniques," *J. Appl. Phys.*, **65**(4), 1484 (1989).

Woodworth, J. R., Riley, M. E., Meister, D. C., Aragon, B. P., Le, M. S. and Sawin, H. H., "Ion Energy and Angular Distributions in Inductively Coupled Radio Frequency Discharges in Argon," *J. Appl. Phys.*, **80**, 1304 (1996).

Woodworth, J. R., Riley, M. E., Miller, P. A., Hebner, G. A. and Hamilton, T. W., "Ion Energy and Angular Distributions in Inductively Driven Radio Frequency Discharges in Chlorine," *J. Appl. Phys.*, **81**, 5950 (1997).